Optics and Lasers in Engineering 134 (2020) 106287

Contents lists available at ScienceDirect

Optics and Lasers in Engineering

journal homepage: www.elsevier.com/locate/optlaseng

# A strain-free semi-kinematic mount for ultra-precision optical systems

Defu Zhang [a,*], Pengzhi Li [b], Wei Xu [a,*], Zongxuan Li [a], Guang Jin [a], Jianguo Zhang [c,*]

[a] Changchun Institute of Optics, Fine Mechanics and Physics, Chinese Academy of Sciences, Changchun 130033, China
[b] The University of Manchester, Manchester, M13 9PL, United Kingdom
[c] State Key Laboratory of Digital Manufacturing Equipment and Technology, School of Mechanical Science and Engineering, Huazhong University of Science and Technology, Wuhan 430074, China

A B S T R A C T

A high-precision and strain-free semi-kinematic mount has been proposed in this research for ultra-precision optical systems. The mount includes three identical feet. Each foot constrains the axial and the tangential direction of the lens motion. Three feet in combination precisely control the six degree-of-freedom (6-DOF) motion of the lens. A strain-free mount of the lens was obtained and the high-precision surface figure of the lens was guaranteed. A prototype of the semi-kinematic mount was developed for the lens with diameter/thickness ratio of 6.73. The surface figure testing of the static mount, the 6-DOF dynamic adjustment and the thermal mount of the lens were carried out. The experimental results show that the surface figure of the static mount is 1.963 nm before adhesion on the feet. With the influence of the shrinkage stress of the epoxy glue, the surface figure of the lens is degenerated to 2.133 nm after adhesion on the feet. When the lens is adjusted 30 μm translation in x/y/z-axis direction or 200 μrad rotation around the x/y/z-axis, respectively, the maximum error of the surface figure is 0.2 nm, which implies the excellent matching character between the developed mount and the 6-DOF adjustment mechanism. Furthermore, with the action of 312 mW thermal load, the surface figure degradation of the lens is less than 0.3 nm in reaching steady state, which indicates the strain-free character of the mount. The experimental results verified the effectiveness of the proposed semi-kinematic mount, as well as its promising applications in ultra-precision optical systems.

## 1. Introduction

The critical dimension of the ultra large scale integration (ULSI) is continuously reducing according to Moore's law [1]. The wavelength of the exposure source has been shortened from 436 nm, 365 nm, and 248 nm to 193 nm and 13.4 nm [2,3]. Recently, optical projection exposure has been the most widely used lithographic method in the development of the ULSI. So much attention has been paid on the extension of the technology. The International Technology Roadmap for Semiconductor (ITRS) released in 2015 shows that the 193 nm immersion lithography with dual/multiple exposure is still the mainstream lithography used in chips mass production of 2xnm and 1xnm nodes [4]. As the key component of the deep ultraviolet lithography (DUVL), the projection lens is one of the most sophisticated optomechanical systems. Its performances directly determine the graph transfer capability of the lithography. The optical system of the projection lenses usually consists of 20–30 optical elements [1,2]. Hence, the wavefront aberration and distortion are important indicators that affect the resolution of the projection lenses. Currently, they are usually less than 10 nm. To satisfy the semiconductor industry's requirements, the demand of improving the lithography resolution continues to be increased. As a result, the numerical aperture (NA) of the projection lenses and the diameter of the optical elements become larger and larger. The wavefront aberration and distortion of the optical system have tolerance requirements on the surface figure of each optical element. The mounting accuracy of the optical elements is seriously required. The root mean square (RMS) value of the surface figure of the optical elements needs to achieve the nanometer level and the positioning accuracy needs to achieve the submicron level. This is a huge challenge for the optical element mounting. In addition, the mounting methods are closely related to the operating modes and the environments within the DUVL projection lenses. The mount should not only meet the requirements of the surface figure and the positioning accuracy, but also compensate for the adverse effects of the external stress fluctuation, the temperature change and the vibration on imaging performance. Therefore, the development of high-precision and strain-free mounting devices is of great significance for the imaging quality of the ultra-precision optical systems, such as lithographic projection lenses.

The lenses in the DUVL system are mounted in a different manner than the mirrors used in telescope. The latter is not limited by the aperture shelter and the layout of the mechanical structure is relatively free. Both a side mount and a back mount can be used [5-8]. In addition, there is no long-time laser irradiation during its work process, hence the surface figure change caused by the thermal load is relatively minor. In DUVL, the surface figure of the lenses subjected to laser radiation needs to be strictly controlled. Recently, typical mounting methods in the DUVL projection lenses include kinematic mount [9,10], semi- kinematic mount [11,12], and elastically averaged mount [13,14].

The kinematic mount assumes that the contact of the mount and the lens with 6-DOF occurs only at infinitesimal points, and any lens with more than six contact points is over-constrained [15]. It assumes that

* Corresponding authors.
*E-mail addresses:* zhangdf@sklao.ac.cn (D. Zhang), xwciomp@126.com (W. Xu), zhangjg@hust.edu.cn (J. Zhang).

https://doi.org/10.1016/j.optlaseng.2020.106287
Received 21 January 2020; Received in revised form 3 June 2020; Accepted 22 June 2020
Available online 2 July 2020

the contact point is infinitely small. Only the normal force of the lens surface can be transmitted, and the shearing and bending moments are not transmitted through the contact point. The Herz contact theory is used to determine the stress of the point contact, however it is usually very high which limits the application of the kinematic mount. Jens et al. [16] proposed a kinematic mount in which three convex pads were bonded on the side of the lens. Each pad was fixed on a flexible mount seat, and each seat constrained the tangential and axial translation of the frame by six flexure hinges. The three mount seats were connected in parallel to form a kinematic mount. However, the mount is too large in size. In order to save radial space, it was embedded in three equally spaced gaps of the frame circumference, which will weak the rigidity of the frame.

The semi-kinematic mount reduces the contact stress by using small contact faces at local mounting points [11,15]. This method needs to ensure the accuracy of the mounting feet. If they are not coplanar, the lens will be deformed. By introducing rotational flexibility at each mounting foot, the coplanar requirement is relaxed. When local rotation occurs between the foot and the mount, a self-aligning effect will be achieved during assembly, which is advantageous to reduce the lens stress caused by the mount. Watson et al. [17] disclosed a semi-kinetic mount whose mounting feet include two types: a radial and an axial flexible mount. The former allowed the element to expand and contract along the radial direction caused by temperature change, and prevented the torsion caused by gravity and vibration. The latter made the gravity distribution uniformly and the lens was not over-constrained along the optical axis direction. The nine mounting feet were evenly distributed along the circumference of the lens. Another advantage of the flexible mount was that the mounting force sensitivity due to machine tolerances was reduced.

The elastically averaged mount can be considered as an extension of semi-kinematic mount [11,15]. The method defines flexures as elements that provide controllable motions. For axisymmetric lenses, the insulation of the external disturbance power is achieved by providing the compliance of the mount in radial direction. The effect of the environmental changing on the flexible mount is reduced. The elastically averaged mount includes a side mount and a bottom mount. When the mounting space around the lens is insufficient, the bottom mount can be used. However, a partial aperture of the lens will be blocked. Yuji [18] proposed an assembled multi-flexible mount seats based on the elastic averaging principle. Each mount seat comprised of an upper compression unit and a lower mount unit. Each compression or mount unit was essentially an L-shaped beam flexure. The horizontal end of the flexure was screwed to the frame and the vertical end was held to the lens. However, the mounting method is complicated to assemble. By the tightening force of the screw, it is difficult to accurately control the deformation amount of the L-shaped flexure and the lens. Dirk et al. [19] designed a monolithic flexible mounting device which employed the elastic averaging principle. Each mount consisted of a pair of mirror-symmetrical mount feet. Each foot was a folded beam flexure that had a curvature close to the lens. It has flexibility both in the axial direction and the radial direction. The deformation of the lens can be reduced by the deformation tolerance of the flexure. Therefore, an approximately strain-free mount was achieved. The mount had a monolithic structure and it was suitable for applications in limited space, such as the window elements mounting in projection lenses. Hence, the kinematic mount and the semi-kinematic mount structure are simple to be manufactured, and the mount surface figure of the lens is repeatable. The disadvantage is that the tri-foil aberration is prone to occur. The elastically averaged mount can ensure the minimum changing of the surface figure caused by the self-weight deformation of the lens, but it requires high processing accuracy and it is difficult to repair in the later stage.

The main contribution of this paper is that a strain-free semi-kinematic mount for ultra-precision optical systems has been proposed. The compliance of the mount can absorb the external stress, which mainly comes from the posture adjusting and the thermal load, and reduce the surface figure degradation of the lens. For a lens with a diameter/thickness ratio of 6.73, a semi-kinematic mount prototype was developed. Furthermore, the static mount, the 6-DOF dynamic adjustment and the thermal mount experiments were carried out. The feasibility has been verified that the lens has a high-precision surface figure. The surface figure is insensitive to the 6-DOF posture adjustment and the laser heat radiation. The mount proposed in this research satisfies the requirements of ultra-precision optical systems, such as DUVL projection lenses.

## 2. Method

### 2.1. Problem description

The working principle of the DUVL projection lenses is shown in Fig. 1(a). A dioptric or catadioptric optical system is commonly used [1]. The maximum diameter of the lenses is about 300 mm. The surface figure and positioning accuracy need to reach nanoscale and tens of nanometers. The first set of the NA0.75 projection lens developed by Changchun Institute of Optics, Fine Mechanics and Physics, Chinese Academy of Sciences (CIOMP) is shown in Fig. 1(b) [20]. The 2-DOF and 3-DOF positioning system are used to correct the aberration. The maximum values of the wavefront aberration and distortion which represented by the fringe Zernike polynomials Z5~Z37 are 5.1 nm and 5.7 nm, respectively. The exposure result of 90 nm dense lines are clearly distinguishable, as shown in Fig. 1(c) [21].

The partial optical system of the NA0.75 projection lens is shown in Fig. 2(a) [22,23]. A plano-concave lens in the optical system is chosen as the research object whose parameters are shown in Fig. 2(b). The lens material is fused silica. The lens has a diameter of 175 mm, a curvature radius of 105 mm, a lens center thickness of 26 mm and an upper clear aperture of 163.6 mm. In our present research, an strain-free mount needs to be designed to minimize the surface figure changing in different operating modes.

### 2.2. Principle of the designed mount

The proposed semi-kinematic mount is shown in Fig. 3(a). It includes a lens, a frame and three mounting feet. The lens is fixed to the frame by three flexible feet, and the feet are evenly spaced at intervals of 120° along the circumference of the frame. The materials of the feet and the frame are both stainless steel with a low thermal expansion coefficient. The feet are fabricated by wire electrical discharge machining (WEDM) which enables size accuracy in the order of micrometers.

The foot consists of four single-axis flexible hinges, which include the y-axis hinges I and II, and the cross-hinges I and II, respectively, as shown in Fig. 3(b). The four hinges in the foot are all beam flexures. Although the width $t$ and the slit radius $r$ in hinges are all the same, the length $l$ is different. The cross-hinges I and II are connected in parallel. And then they are connected in series with the y-axis hinges I and II. Therefore, one spherical joint and one translation joint can be obtained, which have four DOF totally. As a result, one foot limits the tangent and the axis direction of the lens. When the three feet are connected in parallel, the 6-DOF of the lens in three-dimensional(3-D) space can be accurately constrained.

The foot has radial flexibility according to the above mentioned introduction. On one hand, when the lens is with the action of thermal load, the foot can conform to the expansion and contraction of the lens. Hence, the internal stress is reduced and the surface figure can be guaranteed. On the other hand, the lens can keep in the precise alignment with the optical axis. Moreover, when the external vibration is transmitted to the mount, the foot is elastically deformed and an eccentric displacement of the lens is allowed. When these disturbances are removed, the energy stored by the foot makes the lens return to its original position.

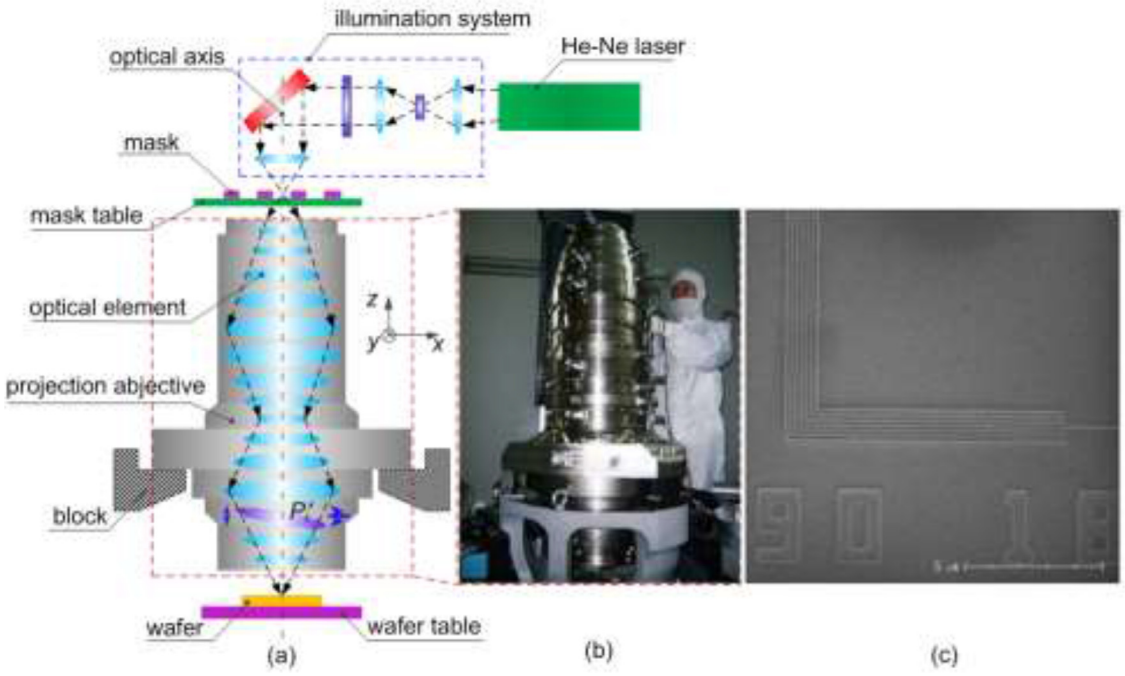


**Fig. 1.** Schematic diagram of the DUVL projection lenses (a)The role of the projection lens (b)The NA0.75 projection lens developed by CIOMP [21] (c)The exposure result of the projection lens [22].

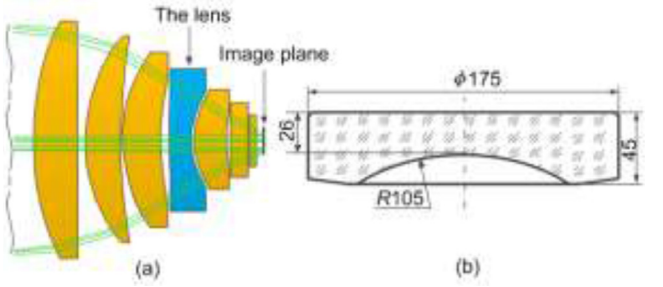


**Fig. 2.** Schematic diagram of the optical system (partly) and the lens (a) The partial optical system (b) The lens's parameters.

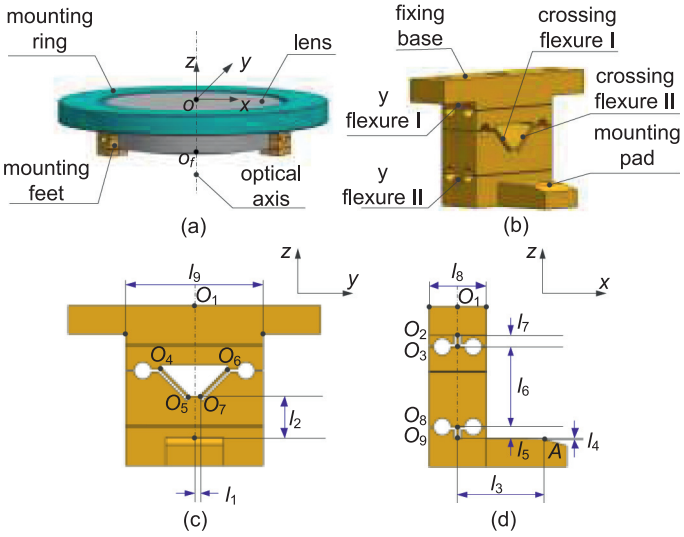


**Fig. 3.** The semi-kinematic mount (a) The assembly of the mount (b) The composition of the foot (c) The main view of the foot (d) The left view of the foot.

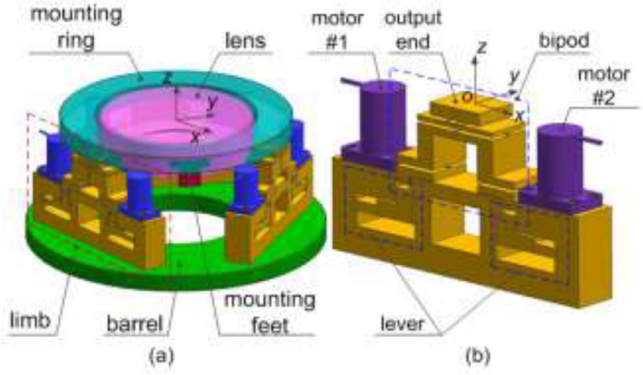


**Fig. 4.** The semi-kinematic mount with 6-DOF posture adjustment (a) The 6-DOF positioning system for the lens (b) The 6-DOF limb.

### 2.3. *Driving force influence on surface figure*

When the lens is disturbed by the external vibration, it may deviate from its ideal position in the optical system. The maximum deviation may be on the order of tens of micrometers. As a result, the lens cannot be returned to its initial position by the flexibility of the passive mount. The active position adjustment device is needed to adjust the posture of the lens, while the surface figure changing of the lens needs to be minimized during the adjusting process. In order to observe the surface figure changing, a 6-DOF posture adjustment system is designed for the proposed semi-kinematic mount, as shown in Fig. 4 [24]. Three identical 6-DOF limbs are distributed around the optical axis at 120° intervals. The upper and lower ends of the limbs are connected to the lower surface of the frame and the common barrel, respectively. Two walking piezoelectric actuators(WPA) are mounted on each limb. The WPA and the levers are connected by flexible hook hinges. When six WPA are controlled to move simultaneously, the mount and the lens can achieve 6-DOF posture adjustment. For clarity, the capacitive dis-

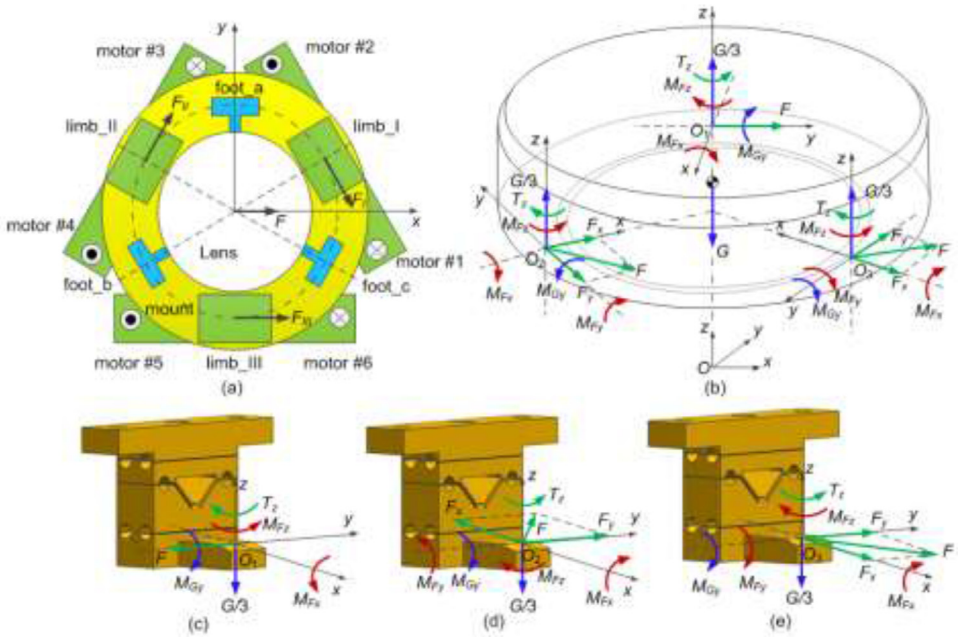


**Fig. 5.** The x-axis translation analysis (a) The driving force (b) The force acting on the lens (c) The force acting on the foot a (d) The force acting on the foot b (e) The force acting on the foot c.

placement sensors used to test the posture of the frame are not shown in Fig. 4.

When the accuracy of lenses surface figure is greatly demanded, the surface figure caused by the driving force cannot be ignored. The matching design between the mount and the 6-DOF adjustment mechanism faces huge challenges. Compared with the passive mounted lens, the surface figure of the lens in the 6-DOF adjustment is not only affected by gravity, but also affected by the driving force. If the surface figure is too sensitive to the driving force, the compensation effect of the image quality will be decreased, and the wavefront aberration of the projection lens cannot be improved. Therefore, it is necessary to study the relationship between the surface figure and the driving force in detail. Recently, the research on the relationship between the driving force and the surface figure is mainly concentrated in the field of active deformable mirrors/lenses [22,25,26]. However, the active optics generally cannot compensate for the positional errors. In addition, the active optics utilizes external driving forces to change the surface figure of the lens, while the 6-DOF posture adjustment needs to reduce the effect of the driving force on the surface figure. Until now, few researches have been carried out to explore the above-mentioned topics.

Taking the x-axis translation adjustment as an example, the influence of the driving force/torque on the surface figure will be qualitatively analyzed. As shown in Fig. 5(a), the push and the pull force directions of the driver are defined as positive (⊙)and negative (⊗), respectively. When carrying out the positive x-axis translation adjustment, drivers #1, #3, and #6 output pull force, and drivers #2, #4, and #5 output push force. The driving force transmission path is introduced as follows. At first, the driving force $F_{\mathrm{I}}$,$F_{\mathrm{II}}$, and $F_{\mathrm{III}}$ act on the frame by the hook hinge, lever, and bipod in each limb. And then the force acts on the lens by the feet, which push the lens to translate forward along the x-axis. Conversely, when drivers #1, #3, and #6 output push force, and drivers #2, #4, and #5 output pull force, then the lens moves negatively along the x-axis.

In addition, the lens is subject to gravity. The total forces and moments acting the lens and the feet are shown in Fig. 5(b) - (e). It can be seen that the driving force and gravity will affect the surface figure of the lens. Due to the magnitude and direction of gravity are constant, the surface figure of the lens changes with the variations of the driving force **F**. Similarly, when the other DOFs of the mount are adjusted, the surface figure also changes with the driving force **F**. Therefore, according to Hooke's law, when the compliance of the feet is constant, the surface figure deterioration of the lens can be reduced by reducing the magnitude of the input driving force.

### 2.4. Driving force influence inhibition

In the 6-DOF adjustment of the lens, there are two main methods for reducing the influence of the driving force on the surface figure which include the driving force isolation and absorption. For a separate lens mount, the driving force isolation only needs to be prevented from being transmitted to the lens. In projection lenses, a cascaded of lens mounts are arranged. The driving force isolation can ensure the surface figure of the current lens, however it may transfer into the other lens in the adjacent mounts, which will result in deterioration of their surface figure. Therefore, this method cannot solve the problem in essence, hence it is not desirable. In addition, the driving force isolation usually needs a part with a relatively high rigidity, which undoubtedly increases the weight, reduces the system mode, and decreases the dynamic performance of the projection lenses. Obviously, this method is contrary to the idea of pursuing the productivity of the ULSI manufacturing.

The most common method is to absorb the driving force. On one hand, the driving force is controlled within an acceptable range by storing energy in flexure hinges. On the other hand, the adoption of the flexible part greatly reduces the weight, optimizes the stiffness distribution, increases the mode of the mount, and improves the dynamic performance of the projection lenses. The designed semi-kinematic mount in this research filters out most of the driving force/torque that will transmit to the lens by the self-deformation of the flexible mount feet. Therefore, the surface figure changing of the lens will be reduced, and the strain-free mount will be achieved.

## 3. Simulation results of posture compensation

By the dynamic posture adjustment of the lens, the compensation effect on the imaging quality of the projection lenses has been analyzed. The lens is considered as a rigid body, and it has 6-DOF in 3-D space. The imaging quality of the projection lenses is sensitive to different DOFs of lenses at different locations in their optical systems. It can be greatly improved by correcting the lens posture using the adjustment mechanism. The x-axis translation adjustment of the lens in the optical system is taken as an example, as shown in Fig. 2. The wavefront aberration

**Table 1**
Material parameters.

| Material | Modulus of elasticity E($\times 10^{10}$Pa) | Poission's ratio $\mu$ | Density $\rho$(kg/m$^3$) | Coefficient of thermal expansion $\alpha$($\times 10^{-6}$/ °C) |
|---|---|---|---|---|
| Fused silica | 7.3 | 0.17 | $2.202 \times 10^3$ | 0.6 |
| Stainless steel 431 | 19.86 | 0.27 | $7.75 \times 10^3$ | 15.6 |

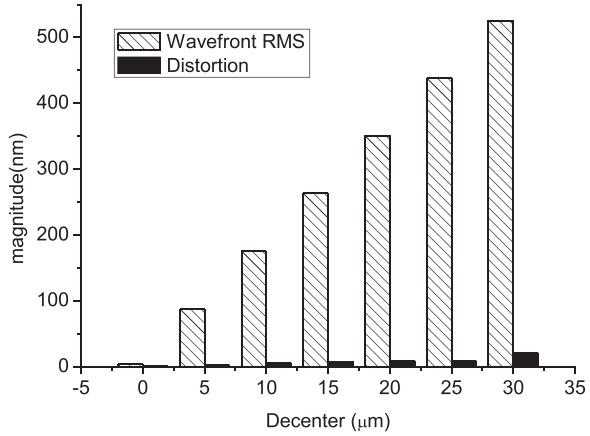


**Fig. 6.** Sensitivity of the wavefront aberration RMS and the distortion to the x-axis positioning errors.

RMS and the distortion are used as evaluation indicators. When the x-axis positioning errors of the lens vary between 5 μm and 30 μm, the maximum values of the wavefront aberration RMS and the distortion of the optical system are introduced in Fig. 6. Both of them increase with the increase of the x-axis displacements, and the wavefront aberration RMS deteriorates faster than the distortion.

The wavefront aberration RMS and the distortion of the optical system without positioning errors are shown in Fig. 7(a) (b). When the eccentric displacement of the lens is 30 μm along the x-axis, the wavefront aberration RMS and the distortion are shown in Fig. 7(c) (d). The maximum value of the wavefront aberration of the field of view changes from 3.575 nm to 525.604 nm, and the distortion changes from 1.179 nm to 20.857 nm. The image quality deteriorates severely.

When the x-axis position error is 30 μm, the x/y-component distortion of the respective field of view points is shown in Fig. 8. The x-component distortion degrades slowly at the center of the rectangular field of view. The degradation rate in the positive and negative x-axis directions increases on the edge of the rectangular field of view. The distortion is substantially unchanged in the y-axis positive and negative directions. The y-component distortion degrades slowly at the center of the rectangular field of view. The degradation rate in both the positive and negative x/y-axis directions accelerates on the edge of the rectangular field of view.

In addition to the x-axis position error, optical elements in projection lenses may also have positional errors in other DOFs. These positional errors can affect the image quality. So the 6-DOF posture adjustment of the lens is necessary for the imaging quality compensation of the projection lenses. A superior mount must has good matching with the adjustment mechanism to ensure the minimal surface figure error caused during the position adjustment. The semi-kinematic mount proposed in this article has been proven to meet the needs.

## 4. Experimental results

In order to verify the performance of the mount proposed in this research, a prototype was developed and tested. The mount material is stainless steel 431, and the lens material is fused silica. The material parameters are shown in Table 1. The assembly process of the lens and the mount is introduced as follows. At first, the position of the feet relative to the frame reference was determined on the coordinate measuring machine (CMM). As following, the frame and the feet were fixed with screws. And then, by adjusting the lens position on the feet, the alignment of the lens and the frame reference was guaranteed. This step was carried out on the centering device. Finally, the feet and the lens were bonded and fixed by epoxy glue. The surface figure was regularly monitored on the interferometer until the changing amount was less than a specified threshold.

### 4.1. Surface figure testing of the static mount

The surface figure of the static mount of the lens was firstly tested, as shown in Fig. 9. The experiment was carried out on a Zygo 12-inch vertical interferometer. Five times measurements were taken and 64 times phase averages were adopted for each testing result. In order to facilitate comparison of the surface figure errors caused by the static mount and the adhesive relative to the initial surface figure, the components of the surface figure are represented by fringe Zernike polynomials and summarized in Fig. 10. The initial surface figure RMS of the lens is 1.362 nm. The main components are pri-spherical aberration (Z9,$n = 4$,$m = 0$) and pri-astigmatism (Z5-Z6,$n = 2$,$m = 2$), which are 1.1 nm and 0.2 nm, respectively. The surface figure of the lens on the semi-kinematic mount before glue is 1.963 nm. It is 2.133 nm after glue which represents the result of the joint action of the static mount and the glue. The larger surface figure errors caused by the static mount and the adhesive are pri-trefoil (Z10-Z11,$n = 3$,$m = 3$) and sec-spherical aberration (Z16,$n = 6$,$m = 0$), which are increased by 1.6 nm and 0.4 nm, respectively. The remaining aberrations caused by the static mount and the adhesive are smaller, and the values are all less than 0.2 nm.

### 4.2. Surface figure testing of the dynamic adjustment

The surface figure of the lens was tested with the proposed 6-DOF dynamic posture adjustment, as shown in Fig. 11 [24]. Each limb of the adjustment mechanism is actuated by two WPA. When six WPA work simultaneously, the mechanism outputs 6-DOF motions. The output motions of the mount are measured by six capacitive displacement sensors. The analog output voltage of the six sensors is changed into digital output by a data acquisition box. Then, the digital output is picked up by a computer through a RS232 interface with a sampling frequency of 10 Hz.

The results of the surface figure in the x-axis translation adjustment are shown in Fig. 12. The initial surface figure before the posture adjustment is 2.023 nm. The error components mainly include pri-trefoil (Z10-Z11), pri-spherical aberration (Z9), and sec-spherical aberration (Z16). The values are 1.7 nm, 0.8 nm, and 0.5 nm, respectively. When the lens is adjusted ±10 μm, ±20 μm, and ±30 μm along the x-axis translation, respectively, the maximum value of the caused surface figure is less than 0.2 nm. The types and values of the error components remain substantially unchanged. It is indicated that the semi-kinematic mount is not sensitive to the driving force, so the mount is well matched with the 6-DOF adjustment mechanism. When the lens returns to its initial position again after the x-axis translation adjustment, the surface figure is 2.077 nm. It substantially does not change relative to the origin value before the x-axis adjustment.

The changing tendency of the surface figure in the x-axis translation adjustment can be observed in Fig. 13. In order to facilitate the comparison of the surface figure variation in different adjustment strokes, the

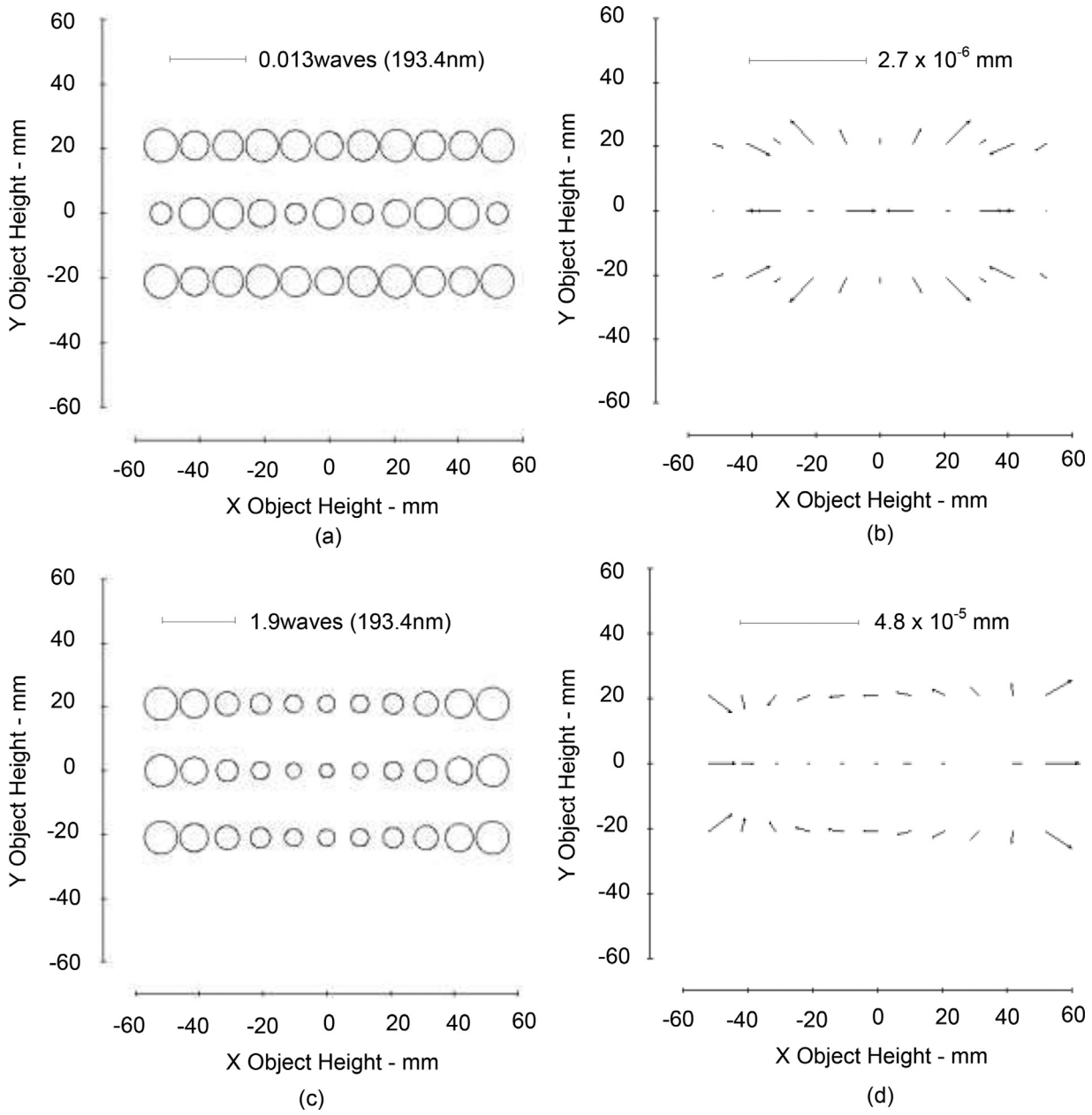


**Fig. 7.** Influence of the x-axis position error on the imaging quality (a) The wavefront aberration when there is no x-axis position error (b) The distortion when there is no x-axis position error c) The wavefront aberration when the x-axis position error is 30 μm (d) The distortion when the x-axis position error is 30 μm.

error components of the surface figure are represented by fringe Zernike polynomial. At first, the relatively large components in the surface figure results are pri-trefoil (Z10-Z11), pri-spherical aberration (Z9), and sec-spherical aberration (Z16), as shown in Fig. 13(a). The values are 1.7 nm, 0.8 nm, and 0.5 nm, respectively. As following, the proportion of various surface figure results does not change with the adjustment stroke. The surface figure errors caused by the x-axis translation adjustment have the following characteristics, as shown in Fig. 13(b). At first, the relatively large components are pri-astigmatism (Z5-Z6) and pri-trefoil (Z10-Z11), respectively. They are 0.2 nm and 0.08 nm, respectively. And then, the proportion of various caused surface figure errors does not change with the adjustment stroke.

Similarly, the y/z-axis translation and the x/y/z-axis rotation experiments have been done. The adjustment displacements are 30 μm/30 μm and 200 μrad/200 μrad/200 μrad. The surface figure results of the lens are 2.071 nm, 2.060 nm, 2.060 nm, 2.055 nm, and 2.062 nm, respectively. The caused surface figure errors are 0.2 nm, 0.177 nm, 0.190 nm, 0.195 nm, and 0.186 nm relative to the initial surface figure, respectively. Therefore, the deterioration of the surface figure with the 6-DOF posture adjustment is small.

### 4.3. Surface figure testing of the thermal mount

The surface figure of the lens with the action of thermal load has been tested. The traditional heating lens method by electric resistance is less efficient, and the heat lost to the surrounding environment is huge [27]. Hence, a high-precision laser infrared heating method was used in this research. In order to simulate the dipole illumination mode of the projection lenses, it is desirable to heat the lens with a dual spot. However, a single spot heating tool which fixes on the Zygo 12-inch vertical interferometer was used in the experiment. The laser spot was used as the input heat source to accurately control the thermal load of the lens. Temperature and surface figure were monitored at the same

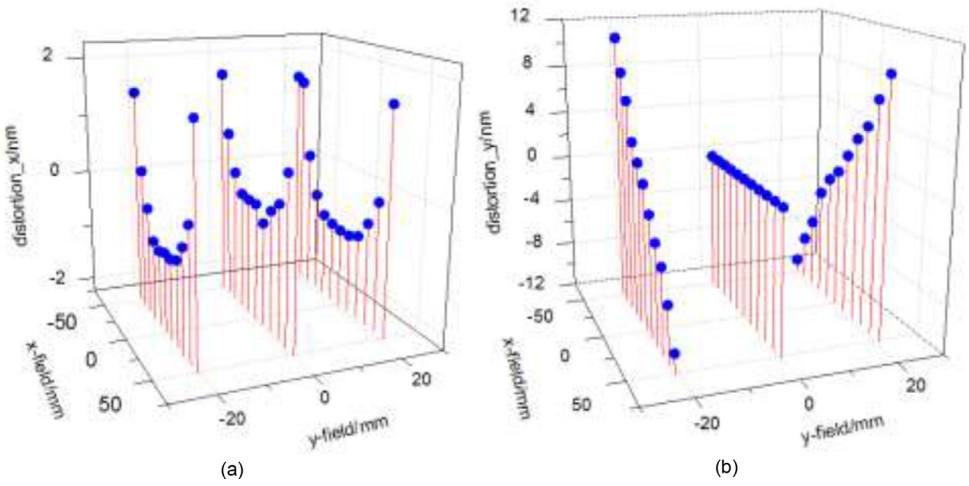


**Fig. 8.** The distortion at respective field of view points. (a) The x-component distortion (b) The y-component distortion.

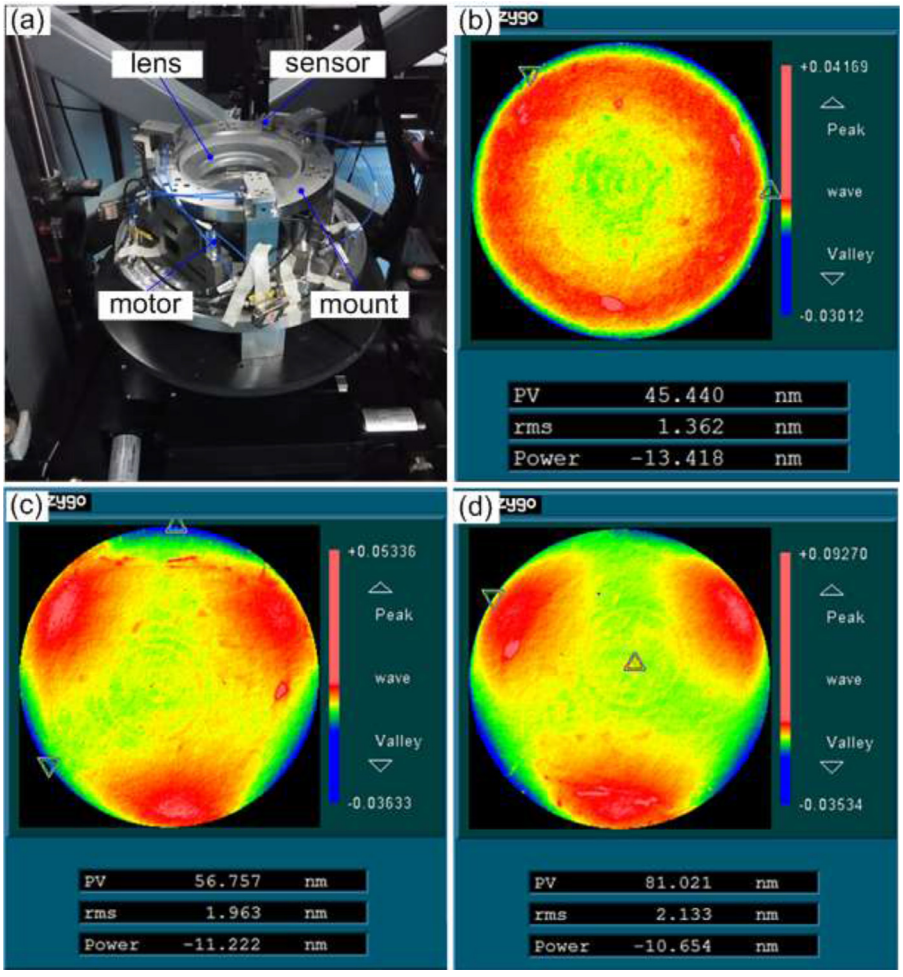


**Fig. 9.** Surface figure errors testing caused by the static mount (a) Surface figure testing system (b) Original surface figure (c) Surface figure before glue on the semi-kinematic mount (d) Surface figure after glue on the semi-kinematic mount.

time. The efficiency of the lens absorbing heat can be improved and the heating error was reduced in the method.

The built thermal testing system is divided into three parts: the laser heating subsystem, the thermal mount subsystem, and the measurement subsystem, as shown in Fig. 14. The laser heating subsystem consists of a laser, a beam splitter, a mirror, an attenuator, a fiber coupler, a solid fiber, a beam expander, and a positioning sleeve. In order to make the heat source uniformly distributed in energy and controllable power on the heating area, a 10.6 μm infrared band $CO_2$ laser was used for heating. Fluke 1594A super-thermometer and Fluke secondary reference thermistor of 5611A-11X silicone-bead probe were adopted as temperature measurement tool. Three 5161A-11X probes were placed on the upper surface of the frame. The temperature of different positions of the frame is measured when the temperature monitoring and the judgment indicators of the system reaching steady state. In the experiment, the average frame temperature when testing the initial surface figure of the mounting subsystem was taken as the initial temperature of the lens. The initial temperature of the frame is 22.153 ˚C. The testing and

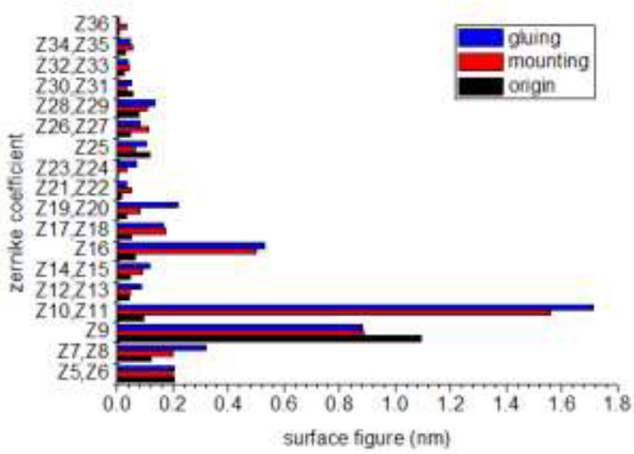


**Fig. 10.** Comparison of the surface figure errors caused by the static mount and the adhesive.

recording started when the laser power and the surface figure of the thermal mount subsystem became stable.

The experimental results are shown in Fig. 15. The results show that when the lens is with the action of the 97 mW thermal load, the steady-state temperature value of the frame is 22.304 ˚C, and the surface figure RMS of the lens is 2.188 nm. When the lens is with the action of the 212 mW thermal load, the frame temperature value is 22.457 ˚C, and the surface figure RMS of the lens is 2.363 nm. When the lens is with the action of the 312 mW thermal load, the frame steady-state temperature value is 22.582 ˚C, and the surface figure RMS of the lens is 2.297 nm. The main error comes from the airflow disturbance on the interferometer measurement. In addition, the laser power stability will also affect the measurement results. In Fig. 15, the error components which increase relative large are pri-astigmatism (Z5-Z6), pri-coma (Z7-Z8,$n$ = 3,$m$ = 1), and pri-spherical aberration (Z9), in which the astigmatism increment is the largest and its value is about 0.5 nm.

## 5. Discussions

According to the experimental results in Section 4.1, the largest component of the surface figure errors is pri-trefoil (Z10-Z11). A solution can be got by combining kinematic mount and gravity compensation mount according to the reference [10], which converts the pri-trefoil (Z10-Z11) into pri-spherical aberration (Z9) firstly. Then the interval between the lenses can be adjusted to eliminate the effects of the spherical aberration. In another method, the pri-trefoil (Z10-Z11) can be eliminated by the active deformation lens [25,26] or the heating lens [27,28]. These two methods are more complex than the method in reference [10]. However, the two methods are more widely used to compensate for the astigmatism caused by the dipole illumination [22]. By increasing the number of heat sources or drivers, they are also possible to compensate for higher-order aberrations. For example, ASML developed the FlexWave active wavefront correction device, which can correct the first 64 terms of the fringe Zernike polynomials, and started to apply the device in the NXT:1950i projection lenses of NA1.35 [29]. Of course, the powerful features also increase the cost and complexity of the optomechanical system.

According to the experimental results in Section 4.1, the surface figure RMS of the lens changed from 1.963 nm to 2.133 nm, and the pri-trefoil (Z10-Z11) reached 1.712 nm when it was fixed on the semi-kinematic mount by glue. The reasons which cause the surface figure to deteriorate are introduced as follows. At first, the thermal expansion coefficient between the epoxy glue and the feet is different. And then, the thickness consistency of the glue layer is difficult to control. In addition, the phenomenon of uneven stress distribution is inevitable inside the lens after glue. To further improve the mounting accuracy of the surface figure, it should be paid more attention to control the bonding stress of the epoxy glue.

Compared with the elastically averaged mount method, the semi-kinematic mount proposed in this research is simple, and the machining process becomes easy. It is not necessary to repair the feet after machining. By the deformation of the mount feet itself, the mount stress inside the lens is reduced, thereby the surface figure of the lens is ensured. The elastically averaged method adjusts the mount stiffness by optimizing the number and size parameters of the feet, so the gravity of the lens is uniformly applied to the feet. Due to the large number of the feet, the surface figure error of the lens is mainly pri-spherical aberration (Z9). When the axial rigidity of the feet is small, it is equivalent to relax the machining accuracy, however the natural frequency of the mount becomes lower. On the contrary, when the axial rigidity of the feet is large, the natural frequency of the mount is improved, and the machining precision requirement is also increased. When the height dimension of the feet is larger than the tolerance which can be trimmed, a large pri-astigmatism (Z5-Z6) will occur. In addition, due to the large number of flexures, the stress release usually undergoes a long-term process, which will result in surface figure drift of the lens.

Compared with the classic kinematic mount [10], bipod needs to be cut from three directions. It needs to be clamped three times which will reduce the machining accuracy. The mount proposed in this article is cut from two directions. It needs to be clamped only twice, which improves the processing precision and efficiency. Furthermore, its volume is more compact than bipod. Therefore, the mount proposed in this research has broad application prospects.

The surface figure is related to the diameter/thickness ratio ($\alpha$) of the lens, in addition to the mechanical mount. The larger the $\alpha$, the more sensitive the lens is to mount. In this research, $\alpha$ equals to 6.73. Using a larger value of $\alpha$ to verify the performance of the mount will be considered subsequently. Considering the position sensitivity in the optical system, the lens in the research was chosen to verify the mount surface figure. In addition to the static mount, the sensitivity of the surface figure to the dynamic posture adjustment has been verified. The

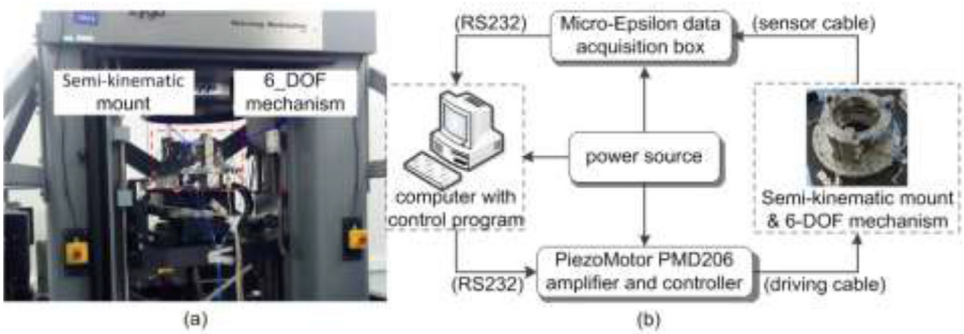


**Fig. 11.** Surface figure testing caused by the 6-DOF dynamic adjustment (a) The experimental setup (b) The hardware connection.

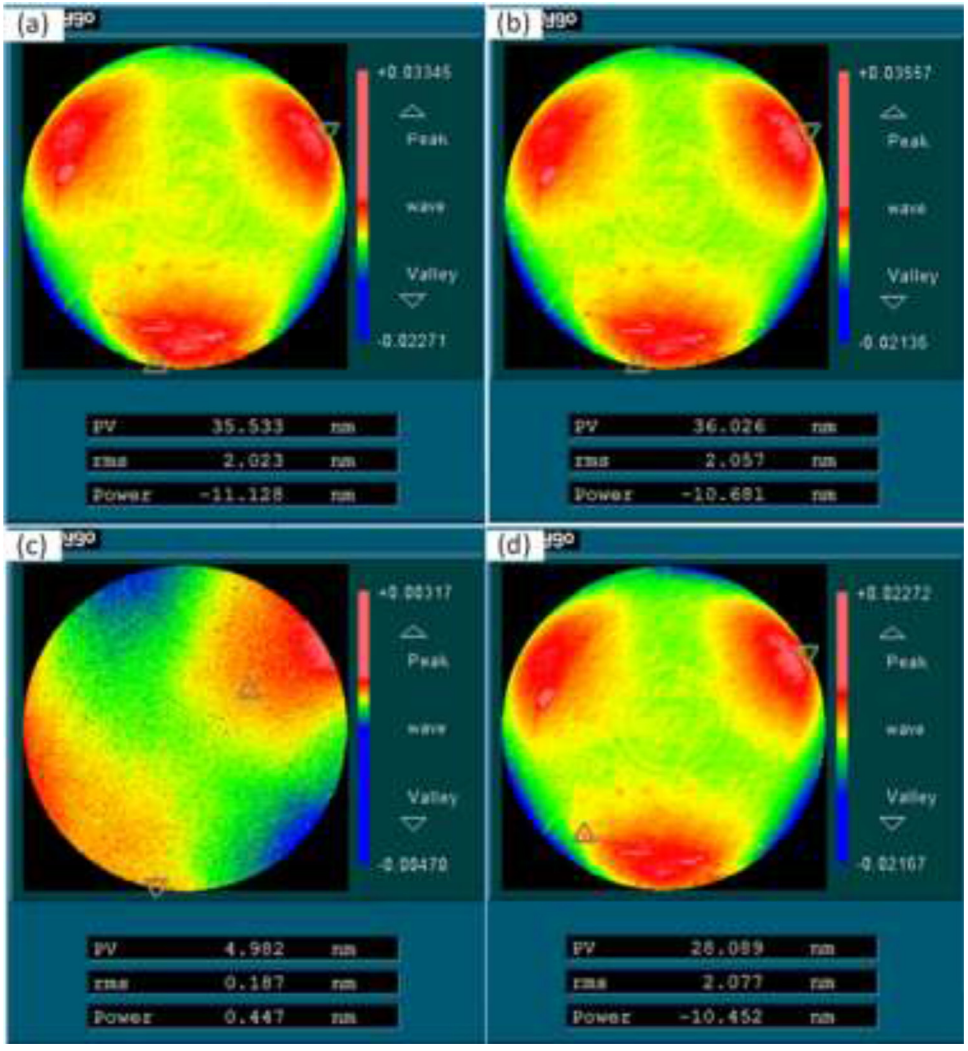


**Fig. 12.** The surface figure results in the x-axis translation adjustment (a) The initial surface figure (b) The surface figure when the x-axis translation adjustment is 30 μm (c) The surface figure change caused when the x-axis translation adjustment is 30 μm (d) The surface figure returning to the initial position.

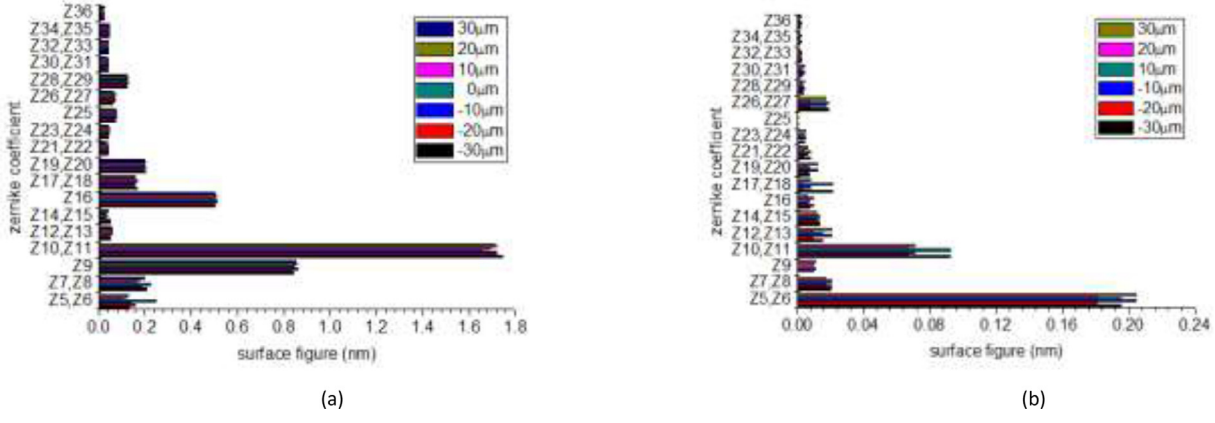


**Fig. 13.** The changing trend of the surface figure by the x-axis translation adjustment (a) The surface figure results after the x-axis translation adjustment (b) The surface figure errors caused by the different x-axis adjustment displacements.

contribution of the 6-DOF posture adjustment to the imaging quality compensation of the optical system was confirmed. According to the analysis results in Section 3, the wavefront aberration RMS and distortion of the optical system increase simultaneously with the position errors of the lens, and the former increases faster. When the position error of the lens is 30 μm in the x-axis direction, the maximum wavefront aberration and the distortion of each field of view of the optical system are degraded by 147 times and 17.7 times, respectively. Although the position error of the lens in x-axis is taken as an example, the lens may have other position errors. Hence, the 6-DOF adjustment is effective for compensating the imaging quality in reality. Therefore, the matching of the strain-free mount with the 6-DOF adjustment mechanism is essential, and it is necessary to control the surface figure deterioration of the lens during posture adjustment. The experimental results show that the

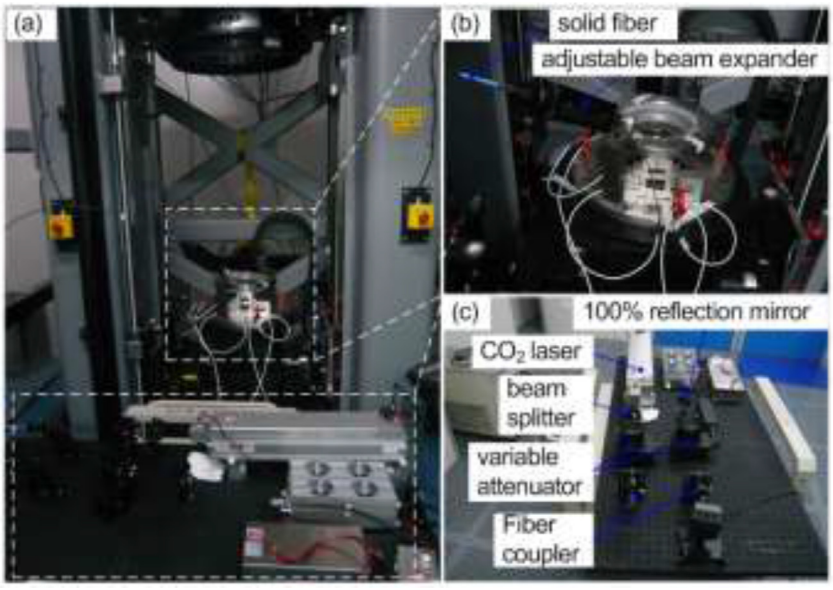


**Fig. 14.** The testing system of the laser heating lens (a) The measurement subsystem (b) The mount subsystem (c) The laser heating subsystem.

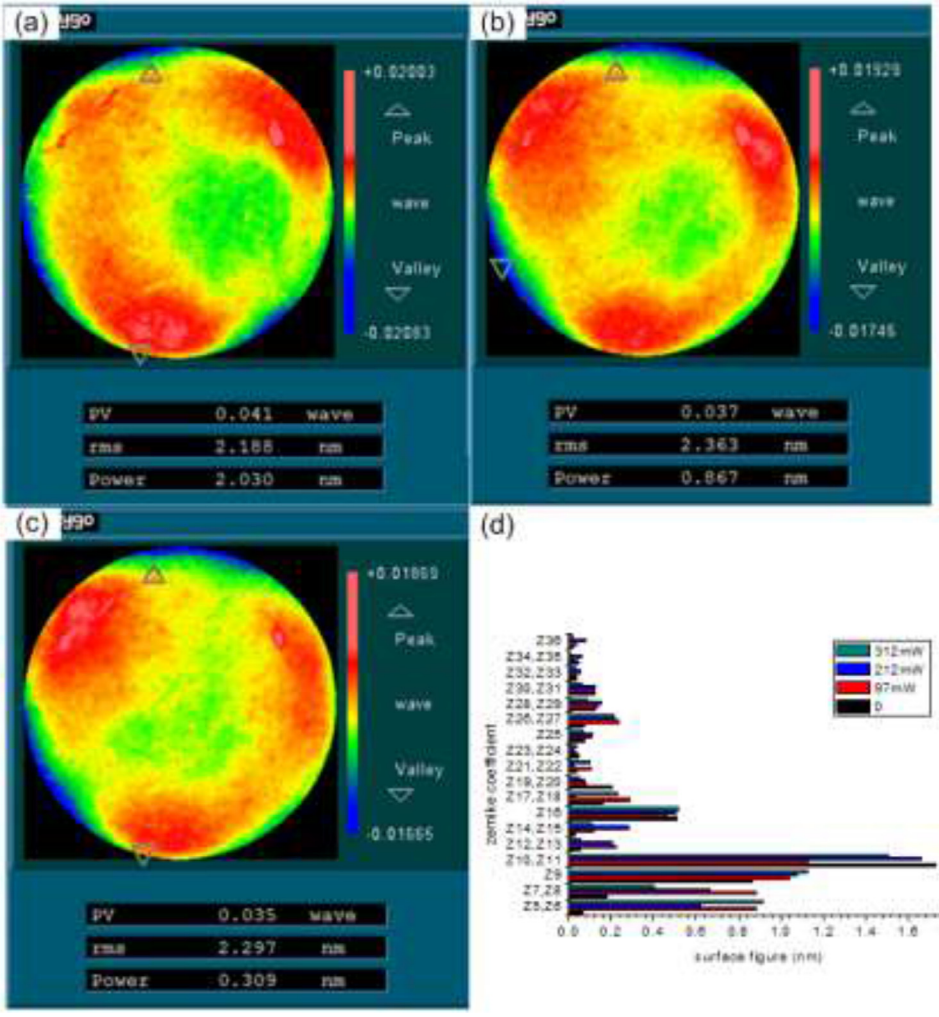


**Fig. 15.** The surface figure results with the action of the different thermal loads (a) The surface figure with the action of the 97 mW thermal load (b) The surface figure with the action of the 212 mW thermal load (c) The surface figure with the action of the 312 mW thermal load.

maximum error of the surface figure is only 0.2 nm when the translation position error of the lens is within 30 μm in x/y/z-axis direction or rotation position error of the lens is within 200 μrad around x/y/z-axis, respectively. It indicates the superiority of the proposed mount.

Different from the posture errors of the lens, the thermal aberration caused by the dipole illumination of the projection lenses cannot be compensated by the posture adjustment. It usually requires compensation by the active deformation mirror/lens [30,31]. Therefore, the mount needs to have a certain degree of thermal load adaptability. The laser heating experiment in Section 4.3 shows that with the action of the 312 mW thermal load, the surface figure degradation of the lens is less than 0.3 nm after reaching the steady state. It indicates that the semi-kinematic mount has a high thermal load stability. On the other hand, it also reflects the rationality of the compliance design of the feet. The feet absorb the thermal expansion deformation of the lens by its own compliance, hence the surface figure deterioration of the lens is reduced.

## 6. Conclusions

A high-precision and strain-free semi-kinematic mount has been proposed for ultra-precision optical systems. The mount includes three identical feet, and each foot constrains the axial and the tangential direction of the lens. Three feet in combination precisely constrain the 6-DOF of the lens. The static mount, the 6-DOF dynamic adjustment, and the thermal mount experiments were performed based on the developed prototype. The mapping relationship between the adjustment displacement and the surface figure of the lens was studied. The influence of the adjustment displacement on aberrations represented by the fringe Zernike polynomials was summarized. The experimental results show that the surface figure of the static mount before the adhesive on the mount is 1.963 nm. The maximum error of the surface figure is only 0.2 nm when the translation position error of the lens is within 30 μm in x/y/z-axis direction or rotation position error of the lens is within 200 μrad around x/y/z-axis, respectively. It reflects a good matching character between the semi-kinematic mount and the 6-DOF adjustment mechanism. With the action of the 312 mW thermal load, the surface figure deterioration is less than 0.3 nm after reaching steady state. The experimental results show that the high-precision mount can absorb external stress, achieve strain-free mount, and reduce the surface figure degradation of the lens. The surface figure of the lens can satisfy the requirements of the DUVL projection lenses. The method provides a reference for the mount and the adjustment mechanism design of the ultra-precision optical systems.

## Funding

National Natural Science Foundation of China (Grant No. 61504142 and 51905194); Science and Technology Development Project of Jilin Province, China (Grant No. C17014, Grant No. 20180414066GH); Wuhan Science and Technology Plan in China (2019010701011400).

## Disclosures

The authors declare no conflicts of interest.

## Declaration of Competing Interest

The authors declare that they have no known competing financial interests or personal relationships that could have appeared to influence the work reported in this paper.

## CRediT authorship contribution statement

**Defu Zhang:** Conceptualization, Methodology, Funding acquisition, Writing - original draft, Writing - review & editing, Resources, Formal analysis, Investigation. **Pengzhi Li:** Software, Data curation, Validation. **Wei Xu:** Writing - review & editing, Resources. **Zongxuan Li:** Writing - review & editing. **Guang Jin:** Writing - review & editing, Supervision. **Jianguo Zhang:** Writing - review & editing, Resources.

## Acknowledgments

We thank Xinfeng Yu, Dongping Wang, Huanan Chen, Jin Li, Liansheng Zhou and Shijun Peng for their support on experiments. The authors gratefully acknowledge the proof reading and valuable comments from the anonymous reviewers.

## References

[1] Lin BJ. Optical lithography: here is why. Bellingham, Washington: SPIE Press; 2010.
[2] Levinson HJ. Principles of lithography. 3rd Edition. Bellingham, Washington: SPIE Press; 2010.
[3] Bakshi V. EUV lithography. Bellingham, Washington: SPIE Press; 2009.
[4] International technology roadmap for semiconductors 2015 edition. http://www.semiconductors.org/main/2015_international_technology_roadmap_for_semiconductors_itrs/
[5] Zhang X, Zhang D, Xu S, Ma H. Active optical alignment of off-axis telescopes based on nodal aberration theory. Opt. Express 2016;24(23):26392–413.
[6] Xu S, Cui Z, Qi B. Compensation factors for 3rd order coma in three mirror anastigmatic (TMA) telescopes. Opt. Express 2018;26(1):298–310.
[7] Yang F, Zhang X, Zhao H, An Q, Guo P, Jiang H, Cao H, Guo P, Luo X, Qi E, HU H, HU H, Zhang J, Chylek T, Cole G, Cho M, Smith B, Campbell M. Relay optical function and pre-construction results of a Giant Steerable Science Mirror for a thirty meter telescope. Opt. Express 2019;27(10):13991–4008.
[8] Han L, Liu C, Fan C, Li Z, Zhang J, Yin X. Low-order aberration correction of the TMT tertiary mirror prototype based on a warping harness. Appl. Opt. 2018;55(7):1662–70.
[9] Yu X, Ni M, Zhang W, Sui Y, Qin S. Analysis and experiments of the thermal-optical performance for a kinematically mounted lens element. Appl. Opt. 2014;53(18):4079–84.
[10] Hale LC. Principles and techniques for designing precision machines," ph.d. dissertation. Cambridge, Massachusetts: Massachusetts Institute of Technology; 1999.
[11] Yoder PR Jr. Opto-Mechanical systems design. 3rd Edition. Bellingham, Washington: SPIE Press; 2006.
[12] Culpepper ML. Design of quasi-kinematic couplings. Precis. Eng. 2004;28:338–57.
[13] Balasubramaniam M, Golaski E, Son S, Sriram K, Slocum A. An anti-backlash two-part shaft coupling with interlocking elastically averaged teeth. Precis. Eng 2002;26:314–30.
[14] Teo TJ, Slocum AH. Principle of elastic averaging for rapid precision design. Precis. Eng 2017;49:146–59.
[15] Vukobratovich D, Richard RM. Flexure mounts for high-resolution optical elements. Proc. SPIE 1988;959:18–36.
[16] K. Jens, W. Ulrich, and S. Dirk, Optical element module with minimized parasitic loads, US Patent, US8351139B2 (2013).
[17] D.C. Watson, and W.T. Novak, Kinematic lens mounting with distributed mount and radial flexure, US Patent, US6239924B1 (2001).
[18] S. Yuji, Correction member, retainer, exposure apparatus, and device fabrication method, US Patent, US6909493B2 (2005).
[19] S. Dirk, W. Andreas, and S. Thomas, Low-deformation mount device of an optical element, US Patent, US7085080B2 (2006).
[20] http://www.cnepo.com.cn/index.php?id=1892
[21] http://www.cnepo.com.cn/index.php?id=1852
[22] Zhao L, Dong L, Yu X, Li P, Qiao Y. Active lens for thermal aberration compensation in lithography lens. Appl. Opt. 2018;57(29):8654–63.
[23] Zhao F, Tang J, Huang W, Xu W. Computer-aided alignment for the lithographic lens[J]. Acta Optica Sinica 2014;34(6):0622001.
[24] Zhang D, Li P, Zhang J, Chen H, Guo K, Ni M. Design and Assessment of a 6-DOF Micro/Nanopositioning System. IEEE/ASME Trans. Mechatronics 2019;24:2097–107.
[25] Lin X, Liu X, Wang J, Wang F, Wei P. Performance test and experiment of correction capability of 137-element deformable mirror. Opt. Precision Eng. 2013;21(2):267–73.
[26] Ahn K, Kihm H. Moment actuator for correcting low-order aberrations of deformable mirrors. OPT LASER ENG 2020;126:105864.
[27] Chen H, Yang H, Yu X, Shi Z. Simulated and experimental study of laser-beam-induced thermal aberrations in precision optical systems. Appl. Opt. 2013;52(18):4370–6.
[28] Schmidt K, Wittmuess P, Piehler S, Ahmed MA, Graf T, Sawodny O. Modeling and simulating the thermoelastic deformation of mirrors using transient multilayer models. Mechatronics 2018;53:168–80.
[29] Staals F, Andryzhyieuskaya A, Bakker H, Beems M, Finders J, Hollink T, Mulkens J, Nachtwein a, Willekers R, Emgblom P, gruner T, Zhang Y. Advanced wavefront engineering for improved imaging and overlay applications on a 1.35 NA immersion scanner. Proc. SPIE 2011;7973:79731G.
[30] Saathof R, Schutten GJM, Spronck JW, Schmidt RHM. Design and characterisation of an active mirror for EUV-lithography. Precis. Eng 2015;41:102–10.
[31] Saathof R, Wansink MV, Hooijkamp EC, Spronck JW, Schmidt RHM. Deformation control of a thermal active mirror. Mechatronics 2016;39:12–27.